CHIN. PHYS. LETT. Vol. 38, No. 7 (2021) 077501 **Express Letter**

Strong Coupled Magnetic and Electric Ordering in Monolayer of Metal Thio(seleno)phosphates

Chenqiang Hua(华陈强)[1], Hua Bai(白桦)[1], Yi Zheng(郑毅)[1], Zhu-An Xu(许祝安)[1], Shengyuan A. Yang(杨声远)[2], Yunhao Lu(陆赟豪)[1*], and Su-Huai Wei(魏苏淮)[3]

[1]*Zhejiang Province Key Laboratory of Quantum Technology and Device, State Key Laboratory of Silicon Materials, Department of Physics, Zhejiang University, Hangzhou 310027, China*

[2]*Research Laboratory for Quantum Materials, Singapore University of Technology and Design, Singapore 487372, Singapore*

[3]*Beijing Computational Science Research Center, Beijing 100193, China*

(Received 6 May 2021; accepted 7 June 2021; published online 18 June 2021)

The coupling between electric ordering and magnetic ordering in two-dimensional (2D) materials is important for both fundamental research of 2D multiferroics and future development of magnetism-based information storage and operation. Here, we introduce a scheme for realizing a magnetic phase transition through the transition of electric ordering. We take $CuMoP_2S_6$ monolayer as an example, which is a member of the large 2D transition-metal chalcogen-phosphates family. Based on first-principles calculations, we find that it is a multiferroic with unprecedented characters, namely, it exhibits two different phases: an antiferroelectric-antiferromagnetic phase and a ferroelectric-ferromagnetic phase, in which the electric and magnetic orderings are strongly coupled. Importantly, the electric polarization is out-of-plane, so the magnetism can be readily switched by using the gate electric field. Our finding reveals a series of 2D multiferroics with special magnetoelectric coupling, which hold great promise for experimental realization and practical applications.

DOI: 10.1088/0256-307X/38/7/077501

Multiferroics, the materials with coexisting ferroelectricity and magnetism, have been a subject of extremely active research in the past twenty years.[1,2] Besides their intriguing fundamental physics, the interest on these materials is highly motivated by their potential for functional device applications, particularly, the prospects of manipulating magnetism purely via electric field, without involving electric currents (which would cause undesired dissipation and heating problems). The multiferroics discovered to date are conventionally classified into two groups.[3] In type-I multiferroics, the ferroelectricity and magnetism have different sources, e.g., originated from different ions, so the coupling between them is typically rather weak. As for type-Ⅱ multiferroics, the ferroelectricity is generated by the magnetism that breaks the inversion symmetry. In this case, the coupling is strong, but the ferroelectricity is generally weak, with low critical temperatures.[4]

The current challenge in multiferroics is to find candidates that can have strong coupling between ferroelectric and magnetic orderings as well as robust ordering. In addition, for device applications, the materials are usually made into layered forms, and it is highly preferred to have out-of-plane electric polarizations such that the orderings can be controlled by using gate electric field.

The advance in two-dimensional (2D) materials opens new possibilities to address this problem. The robust ferroelectric and magnetic orderings have been confirmed in 2D materials in recent few years,[5–9] even some 2D material with multiferroic properties have been proposed.[10–16] The reduced dimension may help to enhance the coupling between different degrees of freedom.[17–19] Indeed, a very recent work predicted that in monolayer $ReWCl_6$, the orientation of the in-plane ferroelectric polarization can exhibit a strong coupling with different magnetic orderings.[20] However, it is technically difficult to control in-plane ferroelectricity, particularly, impossible with gate field. Thus, it remains a challenge to search for strongly coupled multiferroics with out-of-plane ferroelectricity.

In this work, we address this challenge by proposing a scheme to realize 2D strongly coupled multiferroics with out-of-plane electric polarization, which exhibits simultaneous transition in magnetic and electric orderings. Here, different electric orderings couple with different magnetic orderings, and the magnetism is determined by the electric ordering which can be

Supported by the National Key R&D Program of China (Grant No. 2019YFE0112000), the Zhejiang Provincial Natural Science Foundation of China (Grant No. LR21A040001), and the National Natural Science Foundation of China (Grant No. 11974307, 12088101, 11991060, and U1930402).

*Corresponding author. Email: luyh@zju.edu.cn

© 2021 Chinese Physical Society and IOP Publishing Ltd

controlled by gate field [Fig. 1(a)]. Specifically, we will show that there are two phases in our systems, one is the antiferroelectric (AFE)-antiferromagnetic (AFM) phase and the other is the ferroelectric (FE)-ferromagnetic (FM) phase, as shown in Fig. 1(b). Unlike conventional multiferroics, in which the coupling only allows one to tune the magnitude, here, the coupling acts like a logic operation, allowing one to fundamentally change the orderings and to drive a phase transition (Another scenario shown in Fig. S1 in the Supporting Information (SI) with AFE-FM phase and FE-AFM phase may also be realized in certain systems).

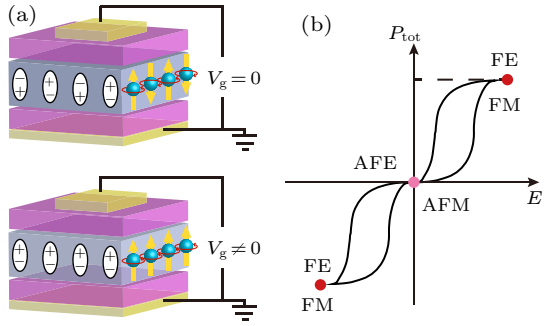

Fig. 1. (a) Schematic diagrams of the magnetic ordering versus electric gate field. Different electric orderings correspond to different magnetic exchange paths and thus result in the different magnetic orderings. (b) P–E loop with the corresponding electric and magnetic ordering.

The idea is motivated by the experimental demonstration of out-of-plane ferroelectricity in 2D few-layered $CuInP_2S_6$.[21] This material belongs to a large family of compounds known as the metal thio(seleno)phosphates (MTPs). MTPs are van der Waals layered materials, with each layer formed by metal cations inserted into a hexagonal $[P_2S(Se)_6]^{4-}$ framework.[22–24] A variety of metal elements and their combinations can be accommodated in this material family, including the transition metals, lanthanide and even actinide elements. Out-of-plane ferroelectricity is common in MTPs containing Cu^{1+} ions, as they tend to be driven by the symmetry-reduction-enhanced strong coupling between occupied Cu $3d$ orbitals and unoccupied s orbitals to deviate from mid-plane of the layer, e.g., as in $CuInP_2S_6$ and $CuInP_2Se_6$.[25,26] Clearly, Cu^{1+} ion with fully filled d-shell is nonmagnetic. To simultaneously have magnetism, besides Cu^{1+}, we may replace the group-Ⅲ metal by a transition metal ion M^{3+}, which is magnetic and has valence +3, to form a quaternary compound $CuMP_2S(Se)_6$, which has been achieved in experiment.[27] From construction, the obtained material should be a type-I multiferroic: the ferroelectricity is from the Cu^{1+} ions, whereas the magnetism is from the M^{3+} ions. Nevertheless, unlike typical type-I multiferroics, we show that in the 2D limit, the polarization of Cu^{1+} ions can strongly affect the magnetic super-exchange interaction between the M^{3+} ions. Taking monolayer $CuMoP_2S_6$ as an example, from first-principles calculations, we find that the change in the electric polarization can even drive a magnetic phase transition: its ground state is (AFE + AFM) ordering; and under a gate electric field, it can be driven into a metastable state which is (FE + FM) ordering. As mentioned above, for conventional multiferroics, the electric control of magnetism is mostly referring to the relatively small change in the magnitude of magnetization or the period of magnetic spirals, etc.[4] This is incomparable with the case here, where the change is in a sense singular as it corresponds to a magnetic phase transition. Thus, we have achieved a truly strongly coupled multiferroic, a breakthrough of both fundamental and practical significances. The 2D character, the out-of-plane electric polarization, and the gate-field control of magnetism endow these new multiferroics with great potential for a wide range of applications.

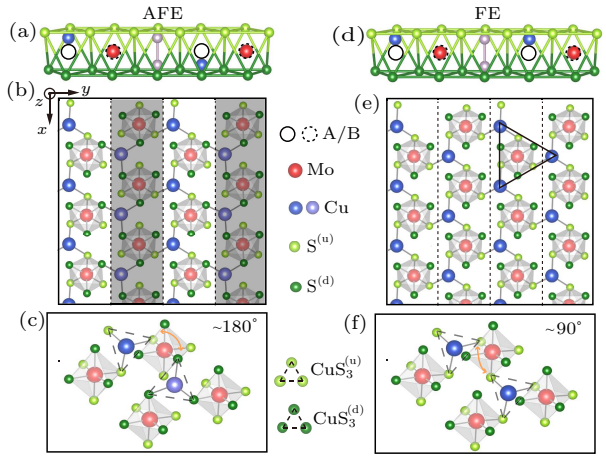

Fig. 2. (a) and (b) The structure of s-AFE $CuMoP_2S_6$. (d) and (e) The structure of FE $CuMoP_2S_6$. In FE, C_3 rotation symmetry (solid triangle) is kept. Mo atoms are represented by red balls and Cu (S) atoms on up/down sides are represented by light/deep blue (green) balls. For high symmetry phase, metals are locating at A/B sites, i.e., the center of MS_6 octahedra. (c) and (f) The perspective view of local octahedral structure at s-AFE state and FE states. The CuS_3 tetrahedral is labeled by dash triangle. P atoms are skipped for clearness.

Let us start by examining the lattice structure of MTP materials. Bulk MTPs have been known for over a hundred years.[22] They are layered materials with layers bonded by weak van der Waals interactions. Hence, 2D MTPs should be readily obtained from the bulk, e.g., by the mechanical exfoliation method, which was indeed demonstrated in recent experiments.[17] Figures 2(a) and 2(d) show the structure of a monolayer MTP in AFE and FE configurations. A common backbone shared by this material family is a hexagonal sublattice of the ethane-like $[P_2X_6]^{4-}$ (X = S, Se) anionic unit. The metal cations

fill the interstitial sites of this framework, which form another honeycomb sublattice. For a quaternary MTP compound, as the $CuMP_2S(Se)_6$ studied here, Cu^{1+} and M^{3+} ions naturally occupy the A and B sites of this honeycomb lattice, as shown in Figs. 2(a) and 2(d).

In this structure, each Cu and M ion is located in an octahedron formed by six surrounding X ions. In a high-symmetry reference state, they should sit at the center of this octahedron. However, as mentioned above, the monovalent Cu^{1+} is known for its tendency towards lower coordination, which is driven by a symmetry-reduction-enhanced coupling between the fully filled $3d^{10}$ orbits and the empty $4s$ orbits.[26,28] As a result, the Cu ions exhibit a sizable vertical shift from the mid plane of the 2D layer. This shift of the Cu ion creates a local electric dipole moment in the out-of-plane direction. It should be mentioned that the M ions generally would display a compensatory shift with the opposite polarity, however, this shift would be much smaller.

To be specific, let us focus on the concrete example $CuMoP_2S_6$ monolayer in the following discussion. In this material, there exists a large shift of Cu from the mid plane. However, the ground state of monolayer $CuMoP_2S_6$ is a stripe type antiferroelectric state in the No. 4 space group. As shown in Figs. 2(a) and 2(b), the Cu ions at neighboring rows undergo shift in opposite directions. The antiferroelectric ground state has no net electric polarization. The similar antiferroelectric ground state has been reported in several MTP materials, such as bulk/layered $CuCrP_2S_6$ and $CuInP_2S(Se)_6$.[21,25,27,29] The ferroelectric state, in which all Cu ions shift in the same direction, corresponds to a metastable state of $CuMoP_2S_6$ ML. In this state, the shift of Cu is about 1.43 Å from the mid plane and the calculated electric dipole is $P = 41.28\,e$Å. Now the space group changes to No. 143, which is quite different from the AFE configuration. Note the instability of the MTP towards AFE and FE states can also be inferred from the phonon spectrum of high symmetry phase (see the SI and Figs. S2 and S3) and the polarization is constrained to be along the out-of-plane (z) direction due to the local C_{3z} rotational symmetry.

In FE structure, the C_3 rotation symmetry constrains all Mo sites with equivalent coordination. While in AFE, due to the striped configuration, this C_3 symmetry is broken, meanwhile, there emerges a glide mirror $G_y = (-x, y + 1/2, 0)$. As already shown in Figs. 2(c) and 2(f), the Cu^+ ions prefer low symmetry structure and shift spontaneously from octahedral center toward three S atoms (dashed triangles) of one side forming CuS_3 tetrahedron. In AFE phase, the CuS_3 tetrahedron locates on opposite sides alternatively [$CuS_3^{(u)}$, $CuS_3^{(d)}$]. As the MoS_6 octahedrons are titled, Mo^{3+} ions connect both up and down S-sublayers [$S^{(u)}$ and $S^{(d)}$] by ~180° $S^{(u)}$–Mo–$S^{(d)}$ geometry [Fig. 2(c)]. On the other hand, the CuS_3 tetrahedron locates on the same side in the FE phase and now, Mo^{3+} in MoS_6 octahedron connects only one S-sublayer by ~90° $S^{(u)}$–Mo–$S^{(u)}$ [or $S^{(d)}$–Mo–$S^{(d)}$] geometry [Fig. 2(f)]. This difference may result in the difference in exchange interactions between AFE and FE.

Next, we turn to the magnetism. In $CuMoP_2S_6$, the magnetism comes mainly from the magnetic moments of the Mo^{3+} ions, which can be clearly visualized from the spin density plot in Figs. 3(a) and 3(c). For the trivalent Mo^{3+} state, there are three remaining electrons occupying the d shell. In the octahedral crystal field from the surrounding S ions, the Mo d orbitals split into the lower t_{2g} and higher e_g orbitals. The three electrons will occupy these t_{2g} orbitals, and according to Hund's rule, they will have parallel spins, leading to a local magnetic moment of $3\mu_B$. This picture is confirmed by our first-principles calculations. For example, it is manifested by the spin-polarized t_{2g} orbitals in the projected band plots in Figs. 3(b) and 3(d). Also, the calculation finds a local moment ~$3\mu_B$ for Mo^{3+} ions.

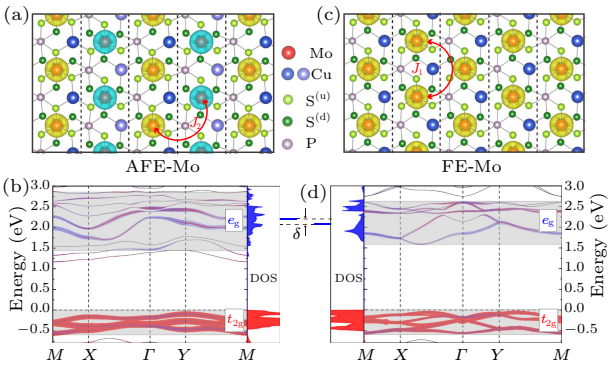

Fig. 3. (a) The structure of s-AFE $CuMoP_2S_6$ monolayer with yellow (blue) color isosurface represents spin-up (spin-down) charge density. (b) The projected band structure and DOS of s-AFE state. (c) The structure of FE $CuMoP_2S_6$ monolayer with spin charge density. (d) The projected band structure and DOS of FE state. The e_g and t_{2g} orbital characters are labeled by blue and red colors, respectively. Note that only spin-up bands are shown here for simplicity. The weight centers of e_g are indicated by blue dashed lines and obviously in s-AFE, the e_g states are broadened in energy resulting in the increase (δ) of exchange gap between t_{2g} and e_g.

Remarkably, the ordering of these magnetic moments is strongly coupled to the electric polarization. In the AFE ground state, the system favors a striped AFM (s-AFM) among several AFM configurations,[30] which conforms to the pattern of the electric ordering [see Fig. 3(a)]; whereas for the FE state, the system prefers the ferromagnetism [see Fig. 3(c)]. Thus, the transition between the two electric states represents a phase transition between (AFE + AFM) and

(FE + FM) orderings. The extremely strong coupling between electric and magnetic orderings revealed here distinguishes the current system from conventional type-I multiferroic materials. In bulk type-I multiferroics such as $BiFeO_3$, the ferroelectricity can tilt the collinear magnetism and form certain long period magnet spirals.[30] In comparison, here the electric polarization even reverses the type of magnetic coupling from AFM to FM. The observation is consistent with the general tendency that couplings between occupied t_{2g}-derived states and unoccupied e_g states are enhanced with reduced dimension. Regarding the magnetic exchange interactions, in 2D, they are mediated by virtual hopping processes confined within the 2D layer, therefore the interaction will have more sensitive dependence on the structural configurations. Hence, the electric ordering transition between FE and AFE corresponds to magnetic ordering transition between FM and AFM.

The well-known Goodenough–Kanamori–Anderson (GKA) rules summarize the dependence of magnetic super-exchange interactions in insulators on some typical lattice configurations.[31–33] Here, the lattice structure is much more complicated and there are multiple exchange paths between the local moments at Mo^{3+} ions. Although it is difficult to give a simple geometric picture like the cases in GKA rules, the first-principles results do indicate that the magnetic super-exchange is strongly affected by the polarization of the Cu^{1+} ions in the 2D layer. This AFE-to-FE transition affects local structure of MoS_6 octahedrons (Table S2) and crystal field of Mo-d orbital. Although the band widths of occupied t_{2g} orbitals for both states are similar, the unoccupied e_g orbitals of magnetic Mo^{3+} ions at FE state are much narrower in energy than the e_g orbitals at AFE state [Figs. 3(b) and 3(d), also see the HSE06 results in Fig. S5] and the split gap between t_{2g} and e_g orbitals is decreased from AFE to FE, also proved by the on-site d levels based on the maximally localized Wannier functions (MLWFs)[34] shown in the SI for details. Thus, exchange virtual gap between the lower t_{2g} and higher e_g orbitals of magnetic ions is reduced by the transition from AFE to FE, which promotes the transition from AFM to FM.

To have a quantitative estimation of the magnetic interaction, we adopt the following classical spin model:

$$H_{\text{spin}} = J_1 \sum_{i,j\in\text{intra}} \boldsymbol{S}_i \cdot \boldsymbol{S}_j + J_2 \sum_{i,j\in\text{inter}} \boldsymbol{S}_i \cdot \boldsymbol{S}_j + K \sum_i (S_i^z)^2 ,$$

where $\boldsymbol{S}_i$ is the normalized local spin at site i, the first and second terms are the exchange interaction between neighboring spins within the same stripe (intra-stripe) and neighboring stripe (inter-stripe), and the third term represents the magnetic anisotropy. The model parameters, including the magnetic exchange couplings J_1, J_2, and the anisotropy strength K, can be extracted from the first-principles calculations via the energy mapping approach. Here, J_1 and J_2 should equal in the ferroelectric state, and they differ in the antiferroelectric state. Importantly, one observes that while the intra-stripe exchange coupling J_1 remains to be FM and is only slightly affected by the electric polarization, the inter-stripe coupling J_2 switches sign between the two states: $J_2(J_1) = -0.25$ meV being FM in the ferroelectric state, and $J_2 = 0.16$ meV being AFM in the AFE state (see Table 1). By Monte Carlo (MC) simulation with anisotropic magnetic energy (see details of anisotropy strength K in the SI Table S4), the critical temperature of magnetic ordering is estimated to be ∼15 K (∼5 K) for FM (AFM) (see Fig. S7).

Table 1. Polarization-dependent effective-exchange interaction J_2 in $CuMP_2X_6$ (M = Cr, Mo or W; X = S or Se).

d^3 (meV)		Cr–S	Mo–S	W–S	Cr–Se	Mo–Se	W–Se
J_2	FE	−1.51	−0.25	3.29	−1.53	0.21	5.54
	AFE	−1.08	0.16	3.82	−0.97	0.62	8.51

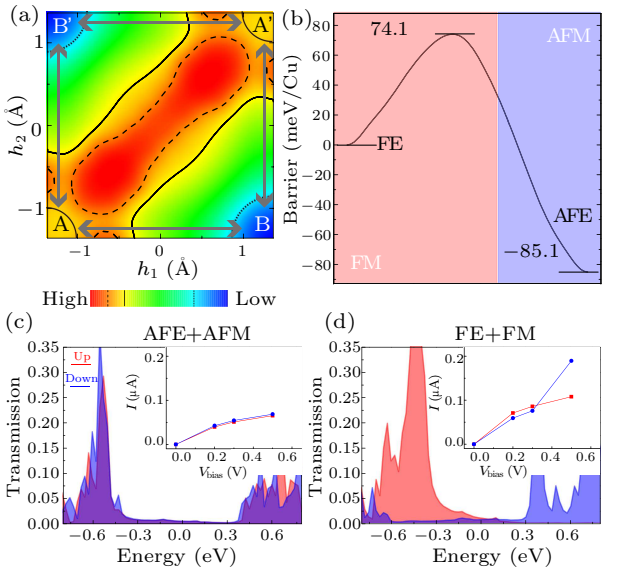

Fig. 4. (a) Energy contour by moving two Cu atoms in the parallel and antiparallel directions. (b) Calculated CINEB barrier between FE and AFE. During the electric transition, the magnetic phase varies from FM to AFM. (c) and (d) Calculated transmission spectrum of $CuMoP_2S_6$ sandwiched by two 2D metallic electrodes under two ordering states (FE + FM and AFE + AFM) with red and blue lines indicating spin-up and spin-down channels, respectively. The insets show the I–V curves of the two spin channels.

Since the polarization is along the out-of-plane direction, this ferroelectric state can be achieved from the ground state by applying a gate electric field. Indeed, we have checked that the system remains insulating during the transition between the AFE and FE states. To investigate the transition

barrier between the (AFE + AFM) and (FE + FM) states, in Fig. 4(a), we plot the free-energy contours for monolayer $CuMoP_2S_6$ in the parameter space of the shifts of Cu ions in neighboring stripes. The two minimum points A and A′ correspond to the (AFE + AFM) ground states. Meanwhile, the two local minima B and B′ give the (FE + FM) metastable states with opposite electric polarizations. We apply the climbing image nudged elastic band method (CINEB)[35] to determine the transition barrier between the A (AFE + AFM) and B (FE + FM) states. The estimated activation energy barrier from A to B is 74.1 meV/f.u. and it is 159.2 meV/f.u. from B to A [Fig. 4(b)]. These values are comparable to the traditional ferroelectric materials such as $PbTiO_3$ (∼200 meV)[36,37] and the 2D ferroelectric In_2Se_3 (66 meV),[5] indicating that an applied gate field can be readily to switch monolayer $CuMoP_2S_6$ from the antiferroelectric ground state to two ferroelectric states (with $\pm P$).

The above analysis can be extended to other 2D materials $CuMP_2S(Se)_6$ in the family, with trivalent magnetic ions M^{3+}, such as Cr and W. The corresponding results are presented in Table 1 and the SI. One can observe that when varying from 3*d* ion Cr^{3+} to 5*d* ion W^{3+}, the enlarged orbital radius tends to enhance the AFM exchange coupling. This is manifested by the observation that $CuCrP_2S_6$ and $CuCrP_2Se_6$ always favor FM ordering, whereas $CuWP_2S_6$ and $CuWP_2Se_6$ always favor the AFM ordering, for both AFE and FE states, although there is obvious change in the inter-stripe exchange coupling strengths (J_2) between the two states. The anion group also affects the exchange interaction. One finds that the change from more localized S-3*p* to relatively delocalized Se-4*p* orbitals promote the AFM exchange interaction. Although for these other materials, the AFE and FE states may not necessarily correspond to different magnetic orderings, the electric polarization does strongly affect the magnetic interaction strengths (Table 1). This also suggests that it should be possible to achieve different magnetic orderings via external perturbations, such as lattice strain. Indeed, we find that a small 2% uniaxial strain is enough to turn the meta-stable state of $CuMoP_2Se_6$ ML from (FE + AFM) to (FE + FM) ordering and the ground state is still (AFE + AFM) ordering, thus it becomes a 2D multiferroic, qualitatively the same as $CuMoP_2S_6$ ML (see Fig. S8).

To elucidate the effects of two ordering states (AFE + AFM and FE + FM) on electron transmission, a tunneling structure with $CuMoP_2S_6$ ML sandwiched by 2D metallic electrodes (ReS_2, see Fig. S9) is constructed. As shown in Figs. 4(c) and 4(d), the transmissions of two spin channels are nearly degenerated for AFE + AFM state. However, the transmission of FE + FM state is largely spin-dependent above and below fermi level, enabling electric control of spin current [inset of Fig. 4(d)]. Although the magnetic orderings remain for other 2D materials $CuMP_2S(Se)_6$, the electric ordering does strongly affect the magnetic interaction strengths and the spin-dependent transmissions of them are also different for the two electric ordering states (Fig. S10). Therefore, $CuMP_2S(Se)_6$ ML provides an ideal platform to the pursuit of controlling magnetism using electric gate at atomic scale.

In summary, we have demonstrated a magnetoelectric effect with logical operation between electric and magnetic orderings and established that the experimentally fabricated MTPs could host such multiferroic properties with out-of-plane polarization (e.g., ML $CuMoP_2S_6$ or stained $CuMoP_2Se_6$). They enjoys the unique property that a gate field can control both its electric polarization and its magnetic ordering. This advantage is of paramount importance for constructing functional devices. For example, it enables magnetic storage that can be controlled purely by gate field without currents. It also enables the magnetic information to be read out through the measurement of electric polarization.

References

[1] Fiebig M, Lottermoser T, Meier D and Trassin M 2016 *Nat. Rev. Mater.* **1** 16046
[2] Zhao W, Fu Z, Deng J, Li S, Han Y, Li M R, Wang X and Hong J 2021 *Chin. Phys. Lett.* **38** 037701
[3] Khomskii D 2009 *Physics* **2** 20
[4] Dong S, Xiang H and Dagotto E 2019 *Natl. Sci. Rev.* **6** 629
[5] Ding W, Zhu J, Wang Z, Gao Y, Xiao D, Gu Y, Zhang Z and Zhu W 2017 *Nat. Commun.* **8** 14956
[6] Wang Y, Xiao C, Chen M, Hua C, Zou J, Wu C, Jiang J, Yang S A, Lu Y and Ji W 2018 *Mater. Horizons* **5** 521
[7] Huang B, Clark G, Navarro-Moratalla E, Klein D R, Cheng R, Seyler K L, Zhong D, Schmidgall E, McGuire M A, Cobden D H, Yao W, Xiao D, Jarillo-Herrero P and Xu X 2017 *Nature* **546** 270
[8] Gong C, Li L, Li Z, Ji H, Stern A, Xia Y, Cao T, Bao W, Wang C, Wang Y, Qiu Z Q, Cava R J, Louie S G, Xia J and Zhang X 2017 *Nature* **546** 265
[9] Xiao C, Wang F, Yang S A, Lu Y, Feng Y and Zhang S 2018 *Adv. Funct. Mater.* **28** 1707383
[10] Huang C, Du Y, Wu H, Xiang H, Deng K and Kan E 2018 *Phys. Rev. Lett.* **120** 147601
[11] Luo W, Xu K and Xiang H 2017 *Phys. Rev. B* **96** 235415
[12] Liu X, Pyatakov A P and Ren W 2020 *Phys. Rev. Lett.* **125** 247601
[13] Gong C, Kim E M, Wang Y, Lee G and Zhang X 2019 *Nat. Commun.* **10** 2657
[14] Li L and Wu M 2017 *ACS Nano* **11** 6382
[15] Xu C, Chen P, Tan H, Yang Y, Xiang H and Bellaiche L 2020 *Phys. Rev. Lett.* **125** 37203
[16] Qi J, Wang H, Chen X and Qian X 2018 *Appl. Phys. Lett.* **113** 043102
[17] Zhang J J, Lin L, Zhang Y, Wu M, Yakobson B I and Dong S 2018 *J. Am. Chem. Soc.* **140** 9768
[18] Zhang J, Shen X, Wang Y, Ji C, Zhou Y, Wang J, Huang F and Lu X 2020 *Phys. Rev. Lett.* **125** 017601
[19] Weng Y, Lin L, Dagotto E and Dong S 2016 *Phys. Rev.*

Lett. **117** 037601
[20] Xu M, Huang C, Li Y, Liu S, Zhong X, Jena P, Kan E and Wang Y 2020 *Phys. Rev. Lett.* **124** 067602
[21] Liu F, You L, Seyler K L, Li X, Yu P, Lin J, Wang X, Zhou J, Wang H, He H, Pantelides S T, Zhou W, Sharma P, Xu X, Ajayan P M, Wang J and Liu Z 2016 *Nat. Commun.* **7** 12357
[22] Susner M A, Chyasnavichyus M, McGuire M A, Ganesh P and Maksymovych P 2017 *Adv. Mater.* **29** 1602852
[23] Burr G, Durand E, Evain M and Brec R 1993 *J. Solid State Chem.* **103** 514
[24] Bourdon X, Maisonneuve V, Cajipe V B, Payen C and Fischer J E 1999 *J. Alloys Compd.* **283** 122
[25] Song W, Fei R and Yang L 2017 *Phys. Rev. B* **96** 235420
[26] Maisonneuve V, Cajipe V, Simon A, Von Der M R and Ravez J 1997 *Phys. Rev. B* **56** 10860
[27] Lai Y, Song Z, Wan Y, Xue M, Wang C, Ye Y, Dai L, Zhang Z, Yang W, Du H and Yang J 2019 *Nanoscale* **11** 5163
[28] Wei S H, Zhang S B and Zunger A 1993 *Phys. Rev. Lett.* **70** 1639
[29] Sun Z Z, Xun W, Jiang L, Zhong J L and Wu Y Z 2019 *J. Phys. D. Appl. Phys.* **52** 465302
[30] Yang J C, He Q, Yu P and Chu Y H 2015 *Annu. Rev. Mater. Res.* **45** 249
[31] Anderson P W 1950 *Phys. Rev.* **79** 350
[32] Goodenough J B 1955 *Phys. Rev.* **100** 564
[33] Kanamori J 1959 *J. Phys. Chem. Solids* **10** 87
[34] Seyler K L, Zhong D, Klein D R, Gao S, Zhang X, Huang B, Navarro-Moratalla E, Yang L, Cobden D H, McGuire M A, Yao W, Xiao D, Jarillo-Herrero P and Xu X 2018 *Nat. Phys.* **14** 277
[35] Sheppard D, Xiao P, Chemelewski W, Johnson D D and Henkelman G 2012 *J. Chem. Phys.* **136** 074103
[36] Cohen R E 1992 *Nature* **358** 136
[37] Yin H M, Zhou H W and Huang Y N 2019 *Chin. Phys. Lett.* **36** 070501

Supporting Information for “Strong Coupled Magnetic and Electric Ordering in Monolayer of Metal Thio(seleno)phosphates”

Chenqiang Hua (华陈强)[1], Hua Bai (白桦)[1], Yi Zheng (郑毅)[1], Zhu-An Xu (许祝安)[1], Shengyuan A. Yang (杨声远)[2], and Yunhao Lu (陆赟豪)[*1], and Su-Huai Wei (魏苏淮)[3]

[1] *Zhejiang Province Key Laboratory of Quantum Technology and Device, State Key Laboratory of Silicon Materials, Department of Physics, Zhejiang University, Hangzhou 310027, China*
[2] *Research Laboratory for Quantum Materials, Singapore University of Technology and Design, Singapore 487372, Singapore*
[3]*Beijing Computational Science Research Center, Beijing 100193, China*

1. Calculation methods

Our first-principles calculations within density functional theory (DFT) framework adopted the projector-augmented wave (PAW)[1] method in the Vienna ab-initio simulation package[2]. We chose Perdew, Burke, and Ernzerhof (PBE)[3] of generalized gradient approximation to describe the exchange-correlation functional and HSE06 has been used to check the results[4]. At least 20 Å vacuum layer is added to avoid unphysical interaction between periodic images along z direction. Energy cutoff was set to be 500 eV for all the calculations. For the rectangular unit cell (Fig. 2), the $10 \times 6 \times 1$ Γ-centered *k*-point mesh was adopted to optimize the structure with 0.005 eV/Å and 10^{-6} eV convergence criterion for force and energy, respectively. While for self-consistent calculations, the mesh was increased to $15 \times 9 \times 1$ and the energy convergence criterion was set to 10^{-7} eV. For the magnetic phase transition, the effect of spin-orbit coupling (SOC) is negligible, which was not included here.

Phonon spectra were calculated based on a 2 × 2 × 1 supercell by the finite displacement method using the PHONOPY package[5]. The spin polarized PBE plus U method was considered in the magnetic calculations[6]: U_{eff} = 1eV for Mo^{3+} (see Fig. S7). Besides, we also check the U_{eff} values for Cr and W MTPs and finally we find there is little influence on our results. The calculations of transmission were performed within the Atomistix toolkit (ATK) package based on the non-equilibrium Green's function (NEGF) approach[7].

2. Simultaneous transition of magnetic and electric orderings

In the main text, we introduce the simultaneous transition of magnetic and electric orderings. One is the transition between antiferroelectric (AFE)-antiferromagnetic (AFM) phase (**P**=0 & **M**=0) and ferroelectric (FE)-ferromagnetic (FM) phase (**P**=1 & **M**=1), as shown in Fig. 1. In Fig. S1(a), the other one is the transition between AFE-FM phase (**P**=0 & **M**=1) and FE-AFM phase (**P**=1& **M**=0), which is another exotic multiferroic transition for application and fundamental research.

3. Spontaneous polarization with vibronic Jahn-Teller effect

When M_1 is equal to M_2, 2D MTPs will represent the fascinating 2D materials, *e.g.* the antiferromagnetic (AFM) $Fe_2P_2S_6$ and $Mn_2P_2Se_6$. From the charge analysis of the antiferromagnetic (AFM) $Fe_2P_2S_6$ and $Mn_2P_2Se_6$, the total valence state of P_2X_6 anion sublattice is about -4, thus on the cation sides, the common combination of oxidation state of two TM ions shall be +1/+3 and +2/+2. Similar to $Fe_2P_2S_6$ and $Mn_2P_2Se_6$,

fully replacing TMs with V^{2+}, Cr^{2+}no spontaneous polarization appear, even with Cr^{2+}/W^{2+} combination. Considering the reported polarized states in $CuInP_2S_6$ by second-order Jahn-Teller effect[8], we can replace In^{3+} with unoccupied *d* electrons such as Cr^{3+} in CrI_3 and keep +1 oxidation state of group IB TM such as Cu^{1+} in the MTP compounds. In CuCl semiconductor[8], when moving toward the anion triangle, the A_1 mode of static Cu increase in energy leading a larger mixing between *s* of and *d* orbital. Similarly in Cu*M*P_2X_6, when Cu moving from the center of octahedra to the face of S triangle (O_h to C_{3v}), the A_1 mode of Cu will transition to the top one from O_h to C_{3v} and this may also contribute to Jahn-Teller effect. Beyond this, from the coordination point of view, the Cu^+ favors low coordination rather than six except the $CuCl_6$ octahedra in $CuCl_2$ crystal.

4. Phonon spectra

It is already reported that there are stripe electric AFE (s-AFE) and FE phases in $CuCrP_2S_6$[9]. To verify both two phases survive when the thickness is diminished to monolayer (ML), we calculate the phonon spectrum of ML $CuCrP_2S_6$ with high symmetry non-polar structure in Fig. S2. From the phonon dispersion, we find the soft optical mode appear at both the Brillouin zone (BZ) center Γ and boundary M, which correspond to the vertical motion of neighboring Cu ions in same/opposite directions, respectively. In Fig. S4(c) and (d), phonon spectrum of FE and AFE are plotted, and all modes are positive, indicating the dynamical stability. Furthermore, we find the phonon spectrum of other ML Cu*M*P_2X_6 has no apparent imaginary phonon modes in

the BZ whether in FE or AFE configuration (Fig. S3).

5. Discussions of magnetism with electric transition

Under the crystal field of MX_6 octagedra, the *d* orbitals will split into two groups: lower t_{2g} and higher e_g manifolds in Fig. S4. For the superexchange interaction, the exchange virtual gap (Δ_c) between two manifolds is one of the important factor to affect the way of magnetic exchange interactions. For example, the d^3 configuration of nearly 90° geometry, the ferromagnetic exchange energy will highly related to virtual gap: $E_{FM} \propto \frac{1}{\Delta_c}$, since the hopping from site 1 to site 2 of e_g manifold costs energy. Therefore, the energy cost may larger than energy gain from parallel exchange interactions under Hund's rules, and thus result in antiparallel configuration (AFM). Although the lattice structure is much more complicated and there are multiple exchange paths between the local moments at M^{3+} ions, we still can find the reduction of exchange virtual gap can enhance the FM interactions from AFE to FE from the projected band structure (Fig. 3 and Fig. S5) and MLWFs on-site energy of *d* orbitals in Table S1. To verify this gap change, we further check the Cr^{3+} systems and find similar gap increase from FE to AFE (see Table S1). The magnetic difference is originated from the geometric difference of Cu ions. In AFE, Cu ions are striped and anti-parallel aligned, leading to the small displacement of Mo ions. Similarly in FE, compensatory displacement also appear. From Table S2, we can readily see the difference from the bond length of Mo-S and angle of S-Mo-S in different configurations. Although other exchange contributions will also influence the ground magnetic state, the trend from AFE to FE in M^{3+} MTPs are consistent with each other

(see Table 1 in main text).

6. Strain manipulation

As discussed in the main text, only ML $CuMoP_2S_6$ is found to be have simultaneous ordering-ordering transition due to contribution of other exchange interactions. However, applying the strain can change the bonding strength (e.g. overlap of the orbitals) and well manipulate the exchange interaction. For example, in Fig. S8, ~ 2% uniaxial strain of ML $CuMoP_2Se_6$ along x or y can tune the magnetic phase in FE and finally achieve the simultaneous ordering-ordering transition as ML $CuMoP_2S_6$.

7. Barrier from CINEB

Based on these monolayer d^3 Cu based MTPs, intriguing magnetoelectric devices can be fabricated. When in AFE ground state, it has low magnetization (AFM or FM). Then the vertical electric field can tune the AFE to FE and thus enlarge the magnetization (stronger FM). Thus for application, the transition barrier between FE and AFE phases needs be investigated by climbing image nudged elastic band method (CINEB)[10]. From AFE to FE, the highest transition barrier is 89.5 meV/Cu in ML $CuMoP_2Se_6$, even lower than ML $CuMoP_2S_6$. Meanwhile, the activation energy barrier for reversal process is 12.1 meV/Cu in Fig. S6. For other MTPs, without lose generality, we calculate the transition barrier of $CuCrP_2Se_6$ as example. In Fig. S6(b), the CINEB determined barrier is quite close to the ML $CuMoP_2Se_6$ with minimal

difference.

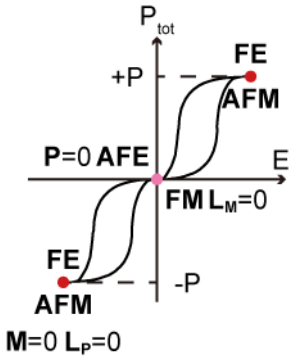

Fig. S1. The FE configuration maintains the AFM state while AFE configuration has FM state. The transition is between AFE-FM phase (P=0 & M=1) and FE-AFM phase (P=1& M=0).

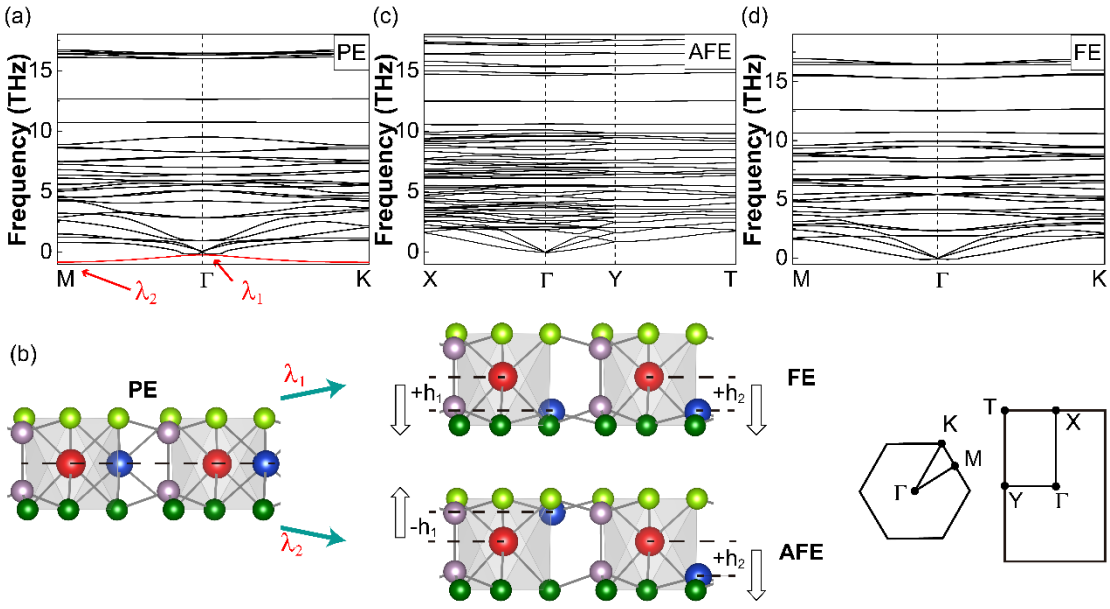

Fig. S2. (a) Phonon spectra of non-polarized monolayer $CuCrP_2S_6$ with soft optical modes. (b) Side views of the different configurations according to soft modes in (a). The height differences between horizontal line and two TM_2 (Cu) are labeled by h_1 and h_2 respectively. (c) – (d) calculated phonon spectrum of AFE and FE $CuCrP_2S_6$ in monolayer limit.

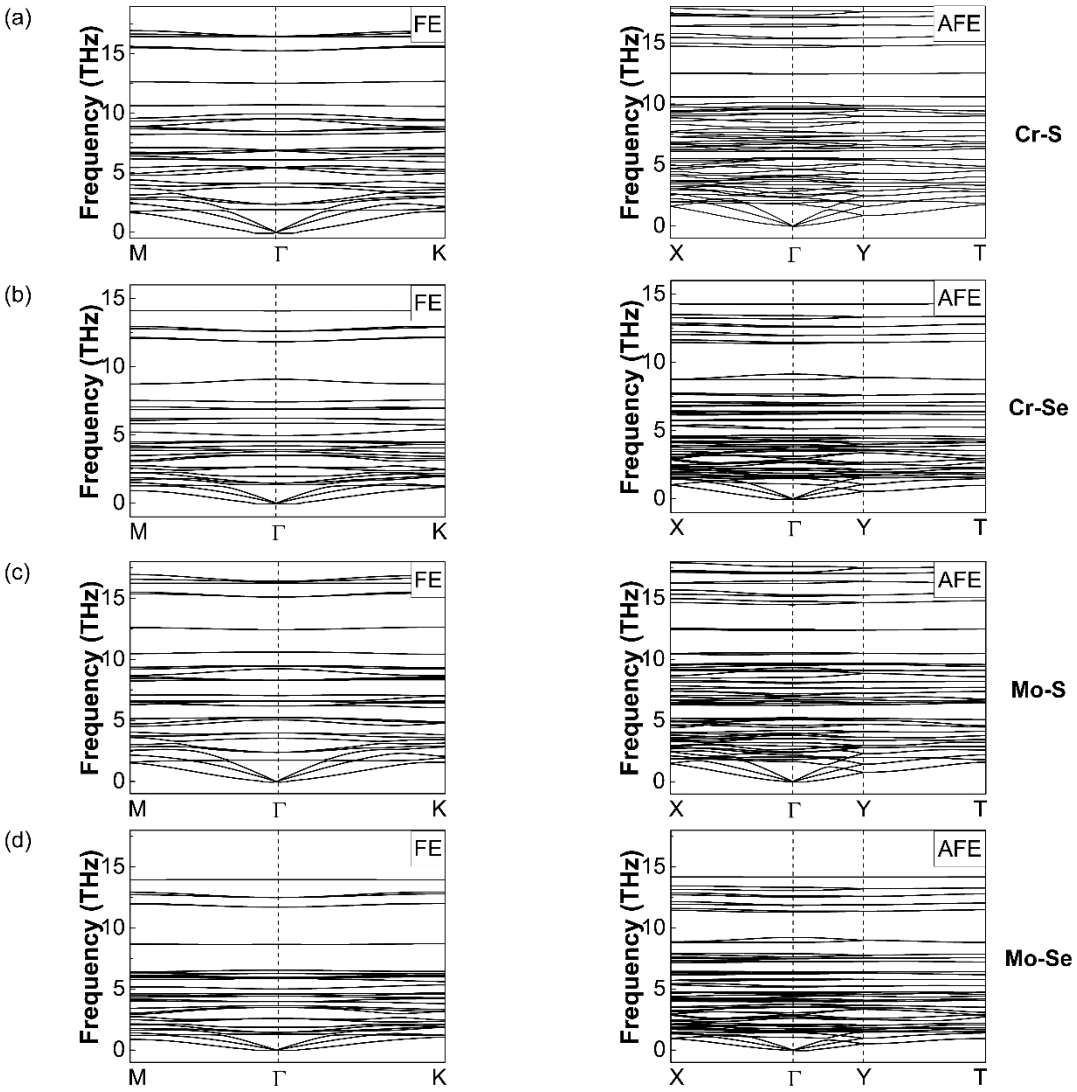

Fig. S3. Phonon spectra of several typical monolayer Cu based MTPs in both AFE and FE configurations. (a) to (d) correspond to Cr-S, Cr-Se, Mo-S and Mo-Se ML systems in both AFE and FE orderings. None of them exhibit obvious imaginary modes in the BZ.

Fig. S4. Under octahedral crystal field, *d* orbitals splitting into t_{2g} and e_g orbitals. Conventionally, the exchange interactions between magnetic ions is highly related to the exchange virtual gap. For example, the hopping from one t_{2g} electron to eg orbitals of another site will cost energy of Δ_c, but follow the Hund's rules, the spin of this electron want to align parallel with spin of t_{2g} electrons. Therefore, the FM or AFM interaction will be the ground state according to the energy competition.

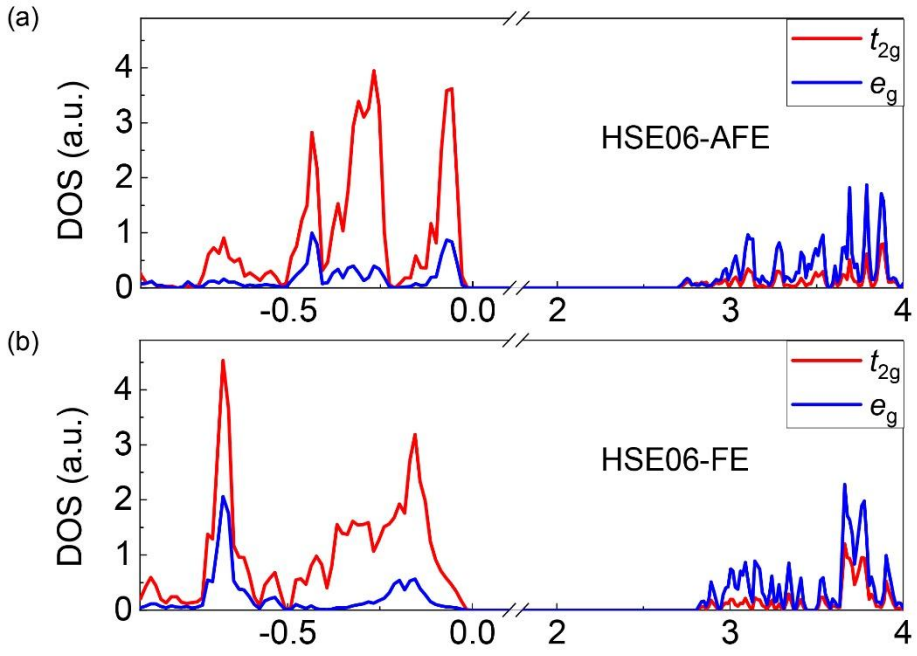

Fig. S5. HSE06 calculated DOS of ML $CuMoP_2S_6$, which is similar to PBE results in the main text Fig. 3. The higher e_g orbitals are also consistent with MLWF energy levels in Table S1.

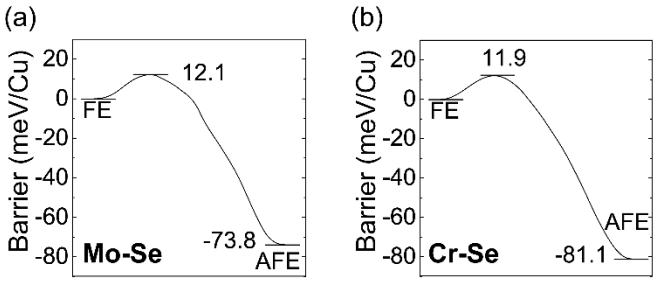

Fig. S6. The calculated barrier between FE and AFE phases of $CuMoP_2Se_6$ by CINEB method. Another plot of calculated barrier of typical system $CuCrP_2Se_6$.

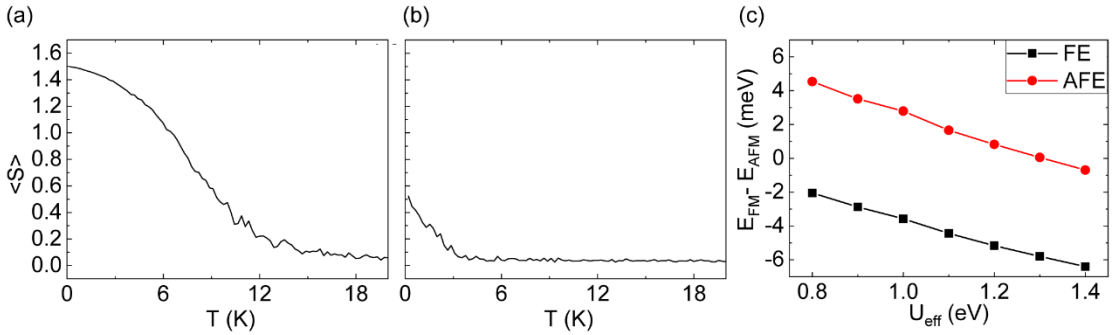

Fig. S7. (a) and (b) Monte Carlo simulation of $CuMoP_2S_6$ FE/AFE monolayer, giving the transition temperature around 15K/5K, defined by the zero averaged spin temperature. (b) Effective Hubbard U_{eff} dependent magnetic phase of $CuMoP_2S_6$ with two electric configurations. Within a large region of U_{eff}, the simultaneous transition of magnetic and electric orderings happen. For the mian results of $CuMoP_2X_6$, the U_{eff} is reasonably set to be 1 eV.

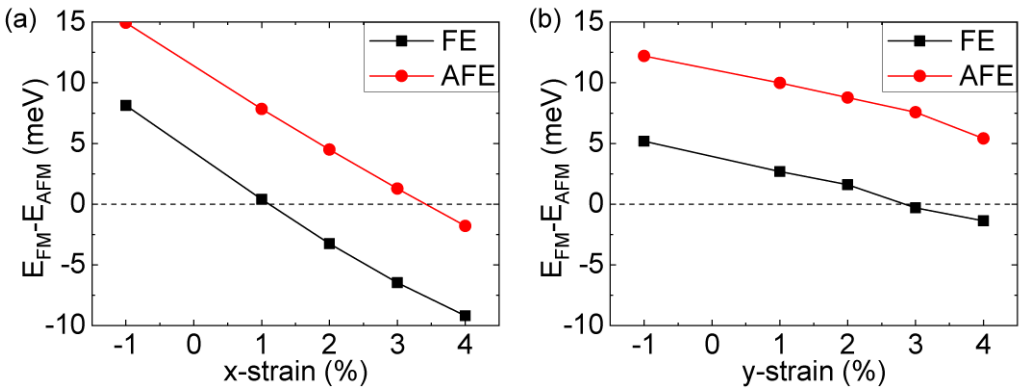

Fig. S8. Uniaxial strain dependent magnetic phase in ML $CuMoP_2Se_6$.

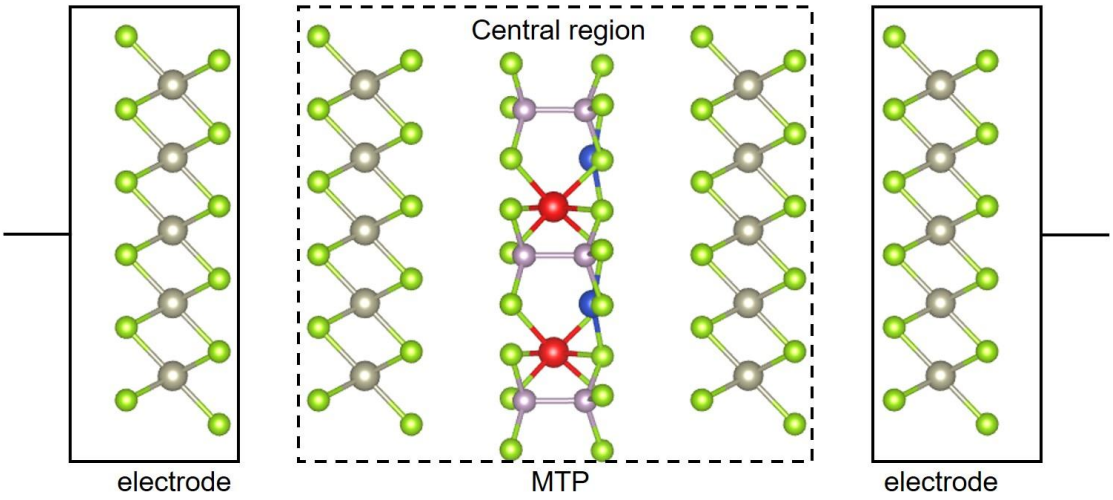

Fig. S9. Schematic figure of MTP based tunneling junction.

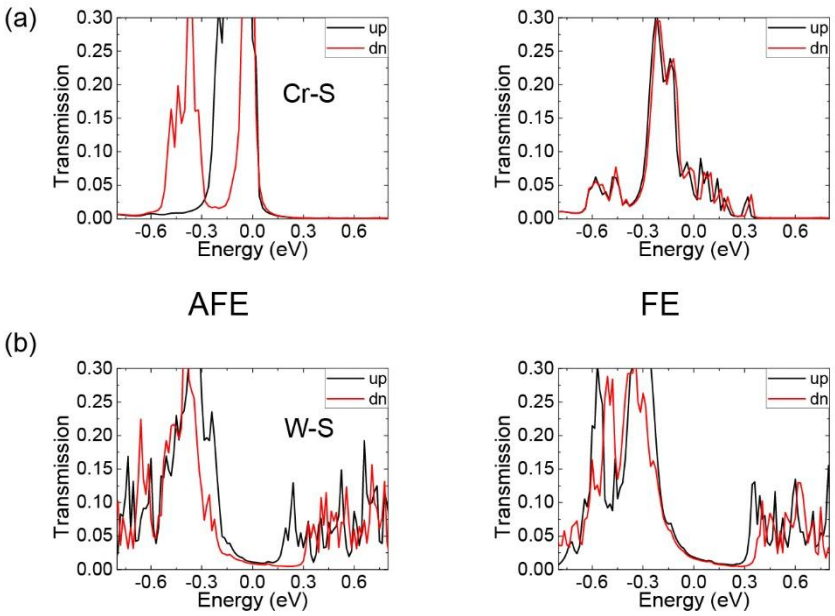

Fig. S10. Calculated transmission spectrum of ML CuCr/WP_2S_6 in both AFE and FE configurations. As expect, the transmission spectrum are nearly degenerated for AFM $CuWP_2S_6$. However, the transmission of FE $CuCrP_2S_6$ doesn't split, which may be originated from the electrode's configuration.

Table S1. MLWFs on-site energy of *d* orbitals: averaged t_{2g} and e_g.

MLWF (eV)	t_{2g}	e_g
Mo-S: FE	0	1.001
Mo-S: AFE	0	1.028
Mo-S: FE-HSE06	0	1.650
Mo-S: AFE-HSE06	0	1.698
Cr-Se: FE	0	1.216
Cr-Se: AFE	0	1.233

Table S2. Bond length and angle in AFE, FE and PE configurations.

Length (Å)	**AFE**	**FE**	**PE**
Mo-$S^{(u)}$	2.537	2.581	2.537
Mo-$S^{(d)}$	2.534	2.496	2.537
Angle (°)	**AFE**	**FE**	**PE**
$S^{(u)}$-Mo-$S^{(u)}$	81.12	78.49	84.64
$S^{(d)}$-Mo-$S^{(d)}$	82.68	85.81	84.64

Table S3. Polarization-dependent effective-exchange-interaction J_1 in Cu$M$$P_2X_6$

d^3 **(meV)**		**Cr-S**	**Mo-S**	**Cr-Se**	**Mo-Se**
J_1	FE	-1.51	-0.25	-1.53	-0.20
	AFE	-0.79	-0.10	-1.24	-0.33

Table S4. Magnetic anisotropy energy (MAE) of $CuMoP_2X_6$, which is defined as E_{001}-E_{100}.

MAE (μeV)	**Mo-S**	**Mo-Se**
FE	637.0	-329.7
AFE	745.0	-301.9

[1] Kresse G and Joubert D 1999 *Phys. Rev. B* **59** 1758–75

[2] Kresse G and Furthmüller J 1996 *Comput. Mater. Sci.* **6** 15–50

[3] Perdew J P, Burke K and Ernzerhof M 1996 *Phys. Rev. Lett.* **77** 3865–8

[4] Tran F and Blaha P 2009 *Phys. Rev. Lett.* **102** 226401

[5] Togo A and Tanaka I 2015 *Scr. Mater.* **108** 1–5

[6] Dudarev S L, Botton G A, Savrasov S Y, Humphreys C J and Sutton A P 1998 *Phys. Rev. B* **57** 1505–9

[7] Brandbyge M, Mozos J-L, Ordejón P, Taylor J and Stokbro K 2002 *Phys. Rev. B* **65** 165401

[8] Wei S-H, Zhang S B and Zunger A 1993 *Phys. Rev. Lett.* **70** 1639–42

[9] Lai Y, Song Z, Wan Y, Xue M, Wang C, Ye Y, Dai L, Zhang Z, Yang W, Du H and Yang J 2019 *Nanoscale* **11** 5163–70

[10] Sheppard D, Xiao P, Chemelewski W, Johnson D D and Henkelman G 2012 *J. Chem. Phys.* **136** 074103